Ladder-based two-dimensional spin model in a radical-Co complex

H. Yamaguchi,[1] Y. Tominaga,[1] A. Matsuo,[2] S. Morota,[1] Y. Hosokoshi,[1] M. Hagiwara,[3] and K. Kindo[2]

[1]*Department of Physical Science, Osaka Metropolitan University, Osaka 599-8531, Japan*

[2]*Institute for Solid State Physics, the University of Tokyo, Chiba 277-8581, Japan*

[3]*Center for Advanced High Magnetic Field Science (AHMF), Graduate School of Science, Osaka University, Osaka 560-0043, Japan*

(Received 3 February 2023; accepted 2 May 2023; published 15 May 2023)

We successfully synthesize a verdazyl-based complex, (p-Py-V-p-F)$_2$[Co(hfac)$_2$]. Molecular-orbital calculations of this complex indicate that spin ladders composed of radical spins are coupled to Co spins via intramolecular interactions, forming a ladder-based two-dimensional (2D) spin model. The complex exhibits paramagnetic behavior associated with Co spins and the 3/5 magnetization plateau; numerical analysis demonstrates that this originates from a rung-singlet-like ground state with fully polarized Co spins. The peculiar behavior of the linear magnetization curve after the magnetization plateau is attributed to the nature of the 2D quantum spin system, which demonstrates a quantum phase transition from the gapped quantum state to the 2D magnetic state. Furthermore, we examine the magnetic anisotropy originating from Co^{2+} in the distorted octahedral environment of the complex. The anisotropic g values are determined by electron-spin resonance (ESR) powder pattern analysis. Considering the spin-orbit coupling and crystal-field distortion of the Co^{2+} ion, we explain the anisotropic g values of the fictitious spin-1/2 on the Co^{2+} ion. We also evaluate the anisotropy of the effective exchange interaction between the radical spin and the fictitious spin on the Co^{2+} ion, thus revealing the existence of an Ising-like exchange interaction.

DOI: 10.1103/PhysRevB.107.174422

I. INTRODUCTION

Spin ladders, as intermediate quantum magnetic systems between one- and two-dimensional spin networks, have attracted considerable attention as a platform for studies relating to field-induced quantum phase transitions (QPTs) and high-temperature superconductors [1,2]. In particular, spin-1/2 antiferromagnetic (AFM) two-leg spin ladders have been extensively studied both theoretically and experimentally. This system forms a rung-singlet state with an energy gap in the excitation spectrum; the subsequent field-induced gapless phase corresponds to a Tomonaga-Luttinger liquid (TLL), which is a quantum critical state with fractional spinon excitations. The ground state of spin ladders varies qualitatively depending on the number of legs; consequently, the spin-1/2 even-leg ladder has a finite energy gap above the ground state, whereas the spin-1/2 odd-leg ladder has no energy gap [3]. As the number of the legs increases, the spin systems becomes equivalent to a two-dimensional (2D) square lattice. Although there is no long-range order for one-dimensional (1D) spin ladders, the square lattice has a Néel order [4]. Spin ladder systems are therefore expected to provide significant insight on the universal dimensional crossover of spin systems associated with the strength of quantum fluctuation.

For spin-1/2 AFM two-leg spin ladders, a QPT between a rung-singlet phase and an ordered phase is expected to occur at a critical value of the interladder coupling J', which depends on the ratio of the leg and rung couplings and the geometry of J'. In the case of a uniform ladder with an intraladder coupling J, the interladder couplings forming a 2D square and a three-dimensional (3D) lattice are expected to show a QPT at $J'/J \approx 0.31$ and 0.11, respectively [5,6]. Furthermore, the effects of frustrated interladder couplings are also extensively studied recently in relation to the reported spin ladder compounds with frustration [7–10].

The verdazyl radical, which is a stable radical with spin-1/2, can be adapted as a ligand for the synthesis of transition-metal complexes [11–15]. In a previous study, we demonstrated that the modulation of the molecular structure of verdazyl radicals enables the design of spin models, realizing unconventional spin-1/2 Heisenberg systems [16–22]. By transforming the verdazyl radicals into ligand structures, we combined the modulated verdazyl radicals with 3d transition metals, leading to the introduction of metal-radical couplings and metal ion magnetic anisotropy into the spin model design [23–29]. Among these, nondirect coordination to the radical center can induce metal-radical exchange couplings on the order of several K, which are suitable for experimental examination of the magnetic-field dependence of the ground state [30,31]. The combination of verdazyl radicals and Co^{2+} ions is expected to produce a variety of Co-containing compounds that pioneer quantum phenomena associated with anisotropic spin systems.

The free Co^{2+} ion, with a d^7 electronic configuration, in an octahedral crystal field has the lowest orbital triplet $^4T_1$. By introducing spin-orbit coupling and crystal-field distortion, the $^4T_1$ ground state can be further split into six Kramers doublets [32,33]. When the temperature is considerably lower than the magnitude of the spin-orbit coupling constant, the effective magnetic moment of Co^{2+} can be described by a fictitious spin-1/2 with anisotropic g values. Furthermore, the effective exchange interactions between fictitious spins are also known to be anisotropic [34–37]. The anisotropy of these interactions strongly depends on the magnitude of the

crystal-field distortion in the Co^{2+} ion, leading to XY- or Ising-like systems.

In this study, we successfully synthesized (p-Py-V-p-F)$_2$[Co(hfac)$_2$] [p-Py-V-p-F = 3-(4-pyridinyl)-1-(4-fluorophenyl)-5-phenylverdazyl, hfac = 1,1,1,5,5,5-hexafluoro-2,4-pentanedione], a Co-verdazyl complex. Molecular-orbital (MO) calculations of this complex indicate that spin ladders composed of radical spins are coupled to Co spins via intramolecular interactions, forming a ladder-based 2D spin model. The magnetization exhibits paramagnetic behavior associated with Co spins and the 3/5 magnetization plateau, indicating the formation of a rung-singlet-like ground state composed of radical spins coupled with fully polarized Co spins. Through numerical analysis, we demonstrate that the almost linear increase in magnetization curve above the plateau phase reflects the two-dimensional nature of the spin system, thereby indicating the existence of interactions between the spins on the verdazyl radicals and the Co^{2+} ion. The anisotropic g values associated with the Co spin are also determined from electron-spin resonance (ESR) powder pattern analysis. Then, considering the spin-orbit coupling and crystal-field distortion of the Co^{2+} ion, we explain the anisotropic g values of the fictitious spin-1/2 on the Co^{2+} ion. The Ising-like exchange interaction between the radical spin and the fictitious spin on the Co^{2+} ions is also revealed from the crystal-field analysis.

II. EXPERIMENTAL

We synthesized p-Py-V-p-F via the conventional procedure for producing the verdazyl radical [38]. A solution of Co(hfac)$_2 \cdot 2H_2O$ (183.2 mg, 0.36 mmol) in 10 ml of heptane was refluxed at 60 °C. A solution of p-Py-V-p-F (199.4 mg, 0.60 mmol) in 4 ml of CH_2Cl_2 was slowly added and stirred for 1 h. After the mixed solution was cooled to room temperature, a dark-green crystalline solid of (p-Py-V-p-F)$_2$[Co(hfac)$_2$] was separated by filtration and washed with heptane. Single crystals were obtained via recrystallization from a mixed solvent of CH_2Cl_2 and ethanol at 10 °C. The x-ray intensity data were collected using a Rigaku XtaLAB Synergy-S. The crystal structure was determined via a direct method using SIR2004 [39] and refined using the SHELXL97 crystal structure refinement program [40]. Structural refinement was carried out using anisotropic and isotropic thermal parameters for the nonhydrogen and hydrogen atoms, respectively. All hydrogen atoms were placed at the calculated ideal positions. The magnetization was measured using a commercial superconducting quantum interference device (SQUID) magnetometer (MPMS-XL, Quantum Design). The diamagnetic contribution calculated using Pascal's method was subtracted from the experimental data. The high-field magnetization at pulsed magnetic fields was measured using a nondestructive pulse magnet at the Institute for Solid State Physics, the University of Tokyo. The ESR measurement was performed using a vector network analyzer (ABmm), superconducting magnet (Oxford Instruments), and laboratory-built cylindrical cavity at Center for Advanced High Magnetic Field Science, Osaka University. All experiments were performed using powder samples. For the ESR measurements, powder samples were mixed with grease to suppress the orientation in the external field direction. Molecular-orbital (MO) calculations were performed using the UB3LYP method as broken-symmetry hybrid density-functional theory calculations with a basis set of 6-31G. All calculations were performed using the GAUSSIAN09 software package. The convergence criterion was set at 10^{-8} hartrees. We employed a conventional evaluation scheme to estimate the intermolecular exchange interactions in the molecular pairs [41]. The quantum Monte Carlo (QMC) code is based on the directed loop algorithm in the stochastic series expansion representation [42]. The calculations was performed for $N = 256$ under the periodic boundary condition, where N denotes the system size. It was confirmed that there is no significant size-dependent effect. All calculations were carried out using the ALPS application [43,44].

TABLE I. Crystallographic data for (p-Py-V-p-F)$_2$[Co(hfac)$_2$].

Formula	$C_{48}H_{32}CoF_{14}N_{10}O_4$
Crystal system	Triclinic
Space group	$P\bar{1}$
Temperature (K)	100
a (Å)	9.0350(6)
b (Å)	11.3575(5)
c (Å)	13.7237(8)
α (degrees)	69.561(5)
β (degrees)	89.941(5)
γ (degrees)	67.236(5)
V (Å^3)	1202.07(12)
Z	1
D_{calc} (g cm^{-3})	1.572
Total reflections	2795
Reflection used	2737
Parameters refined	349
R [$I > 2\sigma(I)$]	0.0365
R_w [$I > 2\sigma(I)$]	0.0919
Goodness of fit	1.042
CCDC	2 249 371

III. RESULTS

A. Crystal structure and spin model

The molecular structure of (p-Py-V-p-F)$_2$[Co(hfac)$_2$] is shown in Fig. 1(a). The verdazyl radical p-Py-V-p-F and Co^{2+} ion have spin values of 1/2 and 3/2, respectively. The crystallographic parameters are summarized in Table I. In the complex, the Co^{2+} ion is coordinated with two p-Py-V-p-F ligands, yielding an octahedral coordination environment. There is an inversion center at the position of the Co atom, and thus, the two radicals in the molecule are crystallographically equivalent. The bond lengths and angles related to the Co atom are listed in Table II. The MO calculations for p-Py-V-p-F indicate that approximately 64% of the total spin density is present on the central ring with four N atoms. While the phenyl and fluorophenyl rings each contribute approximately 17% and 12% of the spin density, respectively, the pyridine ring accounts for less than 8%. Next, we performed MO calculations to evaluate the intermolecular exchange interactions between the radicals, considering the spin-density distribution

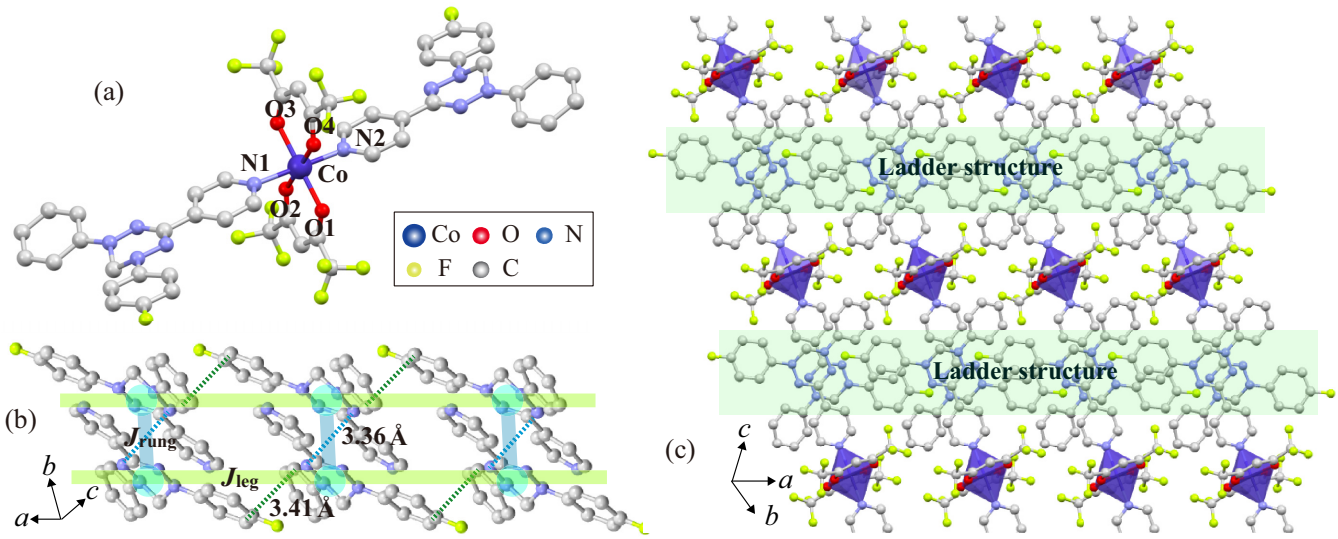

FIG. 1. (a) Molecular structure of (p-Py-V-p-F)$_2$[Co(hfac)$_2$]. The hydrogen atoms have been omitted for clarity. (b) Crystal structure forming the spin ladder composed of neighboring overlapped verdazyl radicals. Each Co(hfac)$_2$ in the molecule has been omitted for clarity. The blue nodes and solid lines represent the S_V of each racial and the intermolecular exchange interactions J_{rung} and J_{leg}, respectively. The dashed lines indicate C–C and N–N short contacts. (c) Crystal structure forming the 2D spin model via intramolecular interactions between spins on the radicals and Co^{2+} ions.

and overlapping of the molecular orbitals. Consequently, we found two predominant AFM interactions forming a spin-1/2 two-leg spin ladder along the a axis, as shown in Fig. 1(b). Their values are evaluated as $J_{rung}/k_B = 64$ K and $J_{leg}/k_B = 12$ K, which are defined in the Heisenberg spin Hamiltonian given by $\mathcal{H} = J_n \sum_{\langle i,j \rangle} S_i \cdot S_j$, where $\sum_{\langle i,j \rangle}$ denotes the sum over neighboring spin pairs. The p-Py-V-p-F pair associated with J_{rung} is related by inversion symmetry and has a N–N short contact of 3.36 Å, yielding a large overlap of the MOs. In terms of J_{leg}, the corresponding p-Py-V-p-F pair is related by translational symmetry and has a C–C short contact of 3.41 Å. The radical-comprised spin ladder structures are connected to the Co^{2+} ions, as shown in Fig. 1(c). Although the intramolecular interactions between the radicals and the Co^{2+} ions are also expected from the molecular structure, reliable evaluations of the $\pi - d$ couplings associated with Co^{2+} ions via MO calculations are difficult. From our previous studies on similar complexes with other transition metals, we expect that the intramolecular exchange interaction J_{Co} is of the order of several K [30,31]. Accordingly, the spins for the verdazyl radicals, S_V, are connected to those of Co^{2+} ions, S_{Co}, via J_{Co}. This results in a ladder-based 2D spin model, as shown in Fig. 2.

TABLE II. Bond distances (Å) and angles (°) related to the Co atom for (p-Py-V-p-F)$_2$[Co(hfac)$_2$].

Co–N1	2.12	O1–Co–O2	89.3
Co–N2	2.12	O2–Co–O3	90.7
Co–O1	2.05	O3–Co–O4	89.3
Co–O2	2.08	O4–Co–O1	90.7
Co–O3	2.05	N1–Co–O4	92.3
Co–O4	2.08	O4–Co–N2	87.7
		N2–Co–O2	92.3
		O2–Co–N1	87.7
		N1–Co–O3	90.8
		O3–Co–N2	89.2
		N2–Co–O1	90.8
		O1–Co–N1	89.2

B. Magnetic properties

Figure 3(a) shows the temperature dependence of magnetic susceptibility ($\chi = M/H$) at 0.1 T. Here, a paramagnetic increase with decreasing temperature is observed. Assuming the formation of the effective spin ladder, S_V spins are expected to form the rung-singlet state with an energy gap. Then, the degree of freedom of S_{Co} spins is considered to remain in the low-temperature region, thus explaining the paramagnetic behavior. The magnetization curves at the low temperatures

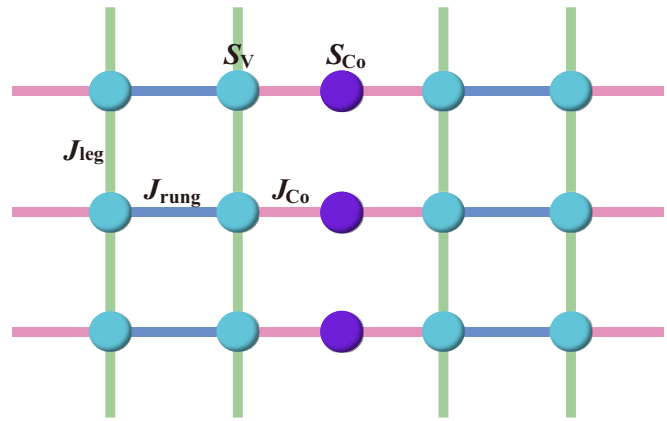

FIG. 2. Ladder-based 2D spin model, illustrating how the spins S_V and S_{Co} (corresponding to the verdazyl radicals and Co^{2+} ions, respectively) are coupled by the intramolecular interaction J_{Co}.

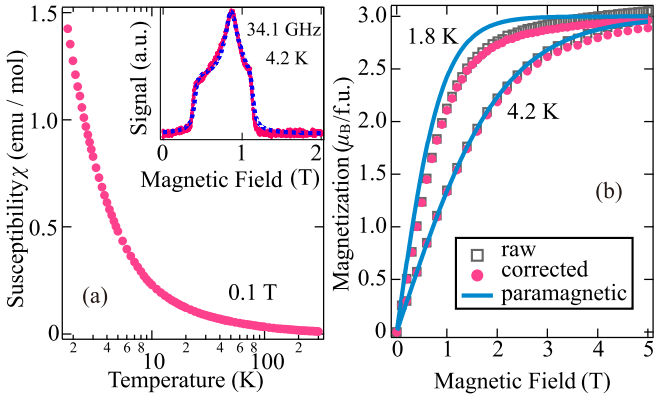

FIG. 3. (a) Temperature dependence of magnetic susceptibility ($\chi = M/H$) of (p-Py-V-p-F)$_2$[Co(hfac)$_2$] at 0.1 T. The inset shows the ESR absorption spectrum of (p-Py-V-p-F)$_2$[Co(hfac)$_2$] at 34.10 GHz and 1.4 K. The broken line represents the powder pattern simulation. (b) Magnetization curves of (p-Py-V-p-F)$_2$[Co(hfac)$_2$] at 1.8 and 4.2 K. The squares denote the raw data, and the circles denote the data as corrected by the subtraction of the Van Vleck paramagnetic term. The solid lines represent the spin-1/2 Brillouin function with $g = 6.0$.

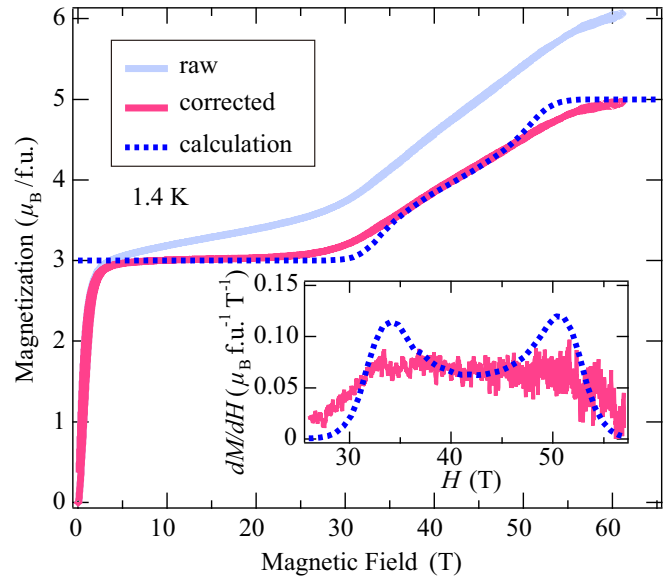

FIG. 4. Magnetization curve of (p-Py-V-p-F)$_2$[Co(hfac)$_2$] at 1.4 K. The corrected data was obtained by subtracting the Van Vleck term from the raw data. The broken line represents the results for the spin ladder ($\alpha = J_{leg}/J_{rung} = 0.17$) as calculated using the QMC method, where the value has been shifted up by 3.0μ_B/f.u. considering the fully polarized S_{Co} spins. The inset shows the corresponding field derivative of the magnetization curve (dM/dH).

also exhibit paramagnetic behavior; this is reminiscent of the Brillouin function, as shown in Fig. 3(b). Here, considering the spin-orbit coupling of Co^{2+} in an octahedral crystal field, the S_{Co} can be described as a fictitious spin-1/2 with anisotropic g values in low-temperature regions. Additionally, the ESR absorption spectrum at 34.10 GHz, as shown in the inset of Fig. 3(a), exhibits broad resonance signals, reflecting the anisotropic g values of the S_{Co} spins. As the powder sample used in the ESR measurement is restrained from orienting along the external field direction by mixing it with grease, the observed signals correspond to the actual powder pattern. The anisotropic g values were evaluated to be between approximately 2.2 and 6.0, as described in the analysis and discussion section. Note that the magnetization curves of the powder samples show asymptotic values of approximately 3.0 μ_B/f.u., which is equivalent to the saturation value of spin-1/2 with $g = 6.0$. Accordingly, it is considered that the powder samples used in the magnetization measurements are oriented in the external field direction owing to the large magnetic anisotropy, leading to the observation of magnetization for the easy axis. The magnetization curves are indeed close to the Brillouin function with $g = 6.0$ along the easy axis, where the Van Vleck term, as evaluated from the high-field magnetization, is subtracted [Fig. 3(b)]. The deviation from the Brillouin function is enhanced with decreasing temperature, indicating the contribution of weak AFM interactions between S_{Co} spins through the triplet excited states of the J_{rung} dimer [17,30].

Figure 4 shows the magnetization curve at 1.4 K in pulsed magnetic fields, where the powder samples are also considered to be oriented in the external field direction. The magnetization assumes a 3/5 plateau for fields in the range 3–25 T, then increases toward saturation at approximately 55 T. The linear increase observed in the plateau phase arises from the temperature-independent Van Vleck paramagnetism of Co^{2+} in the octahedral environment. The evaluated Van Vleck term $\chi_{VV} = 0.018(1)$ μ_B/(Co^{2+} T) is close to the typical values reported previously for Co-based compounds [35,45,46]. The Van Vleck term was then subtracted, and a saturation value of 4.97(4) μ_B/f.u. obtained, which is consistent with the value expected from the molecular unit. The observed plateau indicates the coexistence of the fully polarized S_{Co} spins and a rung-singlet-like gapped state of S_V spins. Meanwhile, the field derivative of the magnetization exhibits an almost linear increase above the plateau phase, as shown in the inset of Fig. 4. This behavior differs from the nonlinear quantum critical behavior of 1D gapped spin systems, where the magnetic field causes a QPT to the TLL phase accompanied by a singular square root behavior in the magnetization curve [18,47–49].

IV. ANALYSES AND DISCUSSION

A. Magnetization curve

We examined the magnetization curve of the present spin model. The MO calculations show that the two-leg AFM spin ladder, which is composed of J_{rung} and J_{leg} ($\alpha = J_{leg}/J_{rung} \simeq 0.19$), are weakly connected by J_{Co}. In the case of $J_{Co} = 0$, the S_V-comprised spin ladder forms a rung-singlet state with an energy gap, resulting in the paramagnetic state of S_{Co} spins. Considering that the experimental results indicate paramagnetic-like behavior of S_{Co} spins, as well as the appearance of a magnetization plateau associated with the energy gap, the present model is expected to have a rung-singlet-like ground state with residual S_{Co} spins. In the high-field region, as the fully polarized S_{Co} spins do not have sufficient degrees of freedom to modify the ground state, the

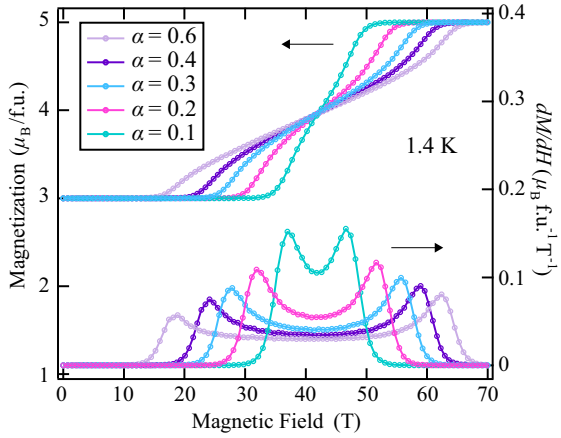

FIG. 5. Calculated magnetization curves for the spin-1/2 spin ladder, and their field derivatives (dM/dH) at 1.4 K for various values of $\alpha = J_{\rm leg}/J_{\rm rung}$.

$S_{\rm V}$-comprised spin ladder is expected to become effective. Accordingly, we calculated the magnetization curve of spin-1/2 spin ladder by using the QMC method. As is often the case with conventional radical compounds, we assumed the Heisenberg spin Hamiltonian and $g = 2.0$. Figure 5 shows the magnetization curves at the experimental temperature for representative values of α, where the magnetic moment of the fully polarized $S_{\rm Co}$ spin is added. The value of $J_{\rm rung}$ was determined for each α to reproduce the intermediate field of the increasing toward saturation, thus equalizing the energy scale. Hence, the $J_{\rm rung}/k_{\rm B}$ values were found to be 54(1) K ($\alpha = 0.1$), 52(1) K ($\alpha = 0.2$), 48(1) K ($\alpha = 0.3$), 45(1) K ($\alpha = 0.4$), and 39(1) K ($\alpha = 0.6$). The increase in α corresponds to an enhancement of one-dimensionality toward the uniform spin ladder, yielding the expansion of the gapless TLL phase as the slopes are reduced. Considering the α dependence, we obtained good agreement between the experimental data and the calculations by using $\alpha = 0.17$ with the parameters $J_{\rm rung}/k_{\rm B} = 52(1)$ K and $J_{\rm leg}/k_{\rm B} = 8.8(2)$ K, as shown in Fig. 4. This confirms that the evaluated values are close to those obtained from the MO calculations. Notably, the field derivative of the calculated magnetization curve exhibits a sharp double-peak structure, which is in clear contrast to the almost linear increase shown in the experimental result. The double-peak structure of dM/dH appears for all α cases and indicates a QPT the TLL phase, which is characteristic of 1D gapped systems. The magnetic behavior in the gapless phase strongly depends on the dimensionality of the basal spin lattice, which is demonstrated by the difference between the isolated system and 1D system in Fig. 5. Thus, the contribution of weak interladder coupling $J_{\rm Co}$ is expected to be more pronounced in the gapless phase. The observed linear increase of the magnetization curve can be attributed to the 2D character due to the interladder couplings. The anisotropic exchange interactions originating from the $S_{\rm Co}$ spins can also cause qualitative difference from assumed Heisenberg system with only $S_{\rm V}$ spin. Accordingly, the peculiar behavior of the linear magnetization after the magnetization plateau is considered to reflect the nature of the current ladder-based model, demonstrating the existence of $J_{\rm Co}$ between the spin ladders. Numerical studies on the effect of interladder couplings indicate that the coupled spin ladder with $\alpha = 0.17$ requires an effective interladder coupling stronger than approximately $0.8J_{\rm rung}$ to stabilize a 2D AFM ordered state [5]. Therefore, considering the energy scale of $J_{\rm Co}$ on the order of several K, the occurrence of the rung-singlet-like state in the present model is consistent with the phase diagram expected in the two-dimensionally coupled spin ladders.

B. Examination of magnetic anisotropy

We simulated the ESR spectra by assuming paramagnetic resonance with anisotropic g values. The ESR powder pattern was obtained by numerically integrating the Lorentzian lineshape, which is expressed as

$$I(H) = \int_0^{2\pi}\int_0^{\pi} \frac{A}{1+[(H-H_{\rm res})/(\Delta H/2)]^2}\sin\theta d\theta d\phi, \tag{1}$$

where $H_{\rm res}$ is the resonance field, ΔH is the linewidth (full width at half maximum), and A is the signal intensity. The angular dependencies of $H_{\rm res}$, ΔH, and A can be expressed using the diagonal components of the principal axes and are given by

$$H_{\rm res} = \frac{h\nu}{\mu_{\rm B}\sqrt{g_x^2\sin^2\theta\cos^2\phi + g_y^2\sin^2\theta\sin^2\phi + g_z^2\cos^2\theta}}, \tag{2}$$

$$\Delta H = \sqrt{\Delta H_x^2\sin^2\theta\cos^2\phi + \Delta H_y^2\sin^2\theta\sin^2\phi + \Delta H_z^2\cos^2\theta}, \tag{3}$$

$$A = \frac{1}{\sqrt{A_x^2\sin^2\theta\cos^2\phi + A_y^2\sin^2\theta\sin^2\phi + A_z^2\cos^2\theta}}, \tag{4}$$

where h is the Planck constant, and ν is the measurement frequency. We explained the observed lineshape using $g_x = 2.18(3)$, $g_y = 2.88(3)$, and $g_z = 6.00(3)$, as shown in the inset of Fig. 3(a). In terms of ΔH and A, we evaluated $\Delta H_x = 0.053(2)$ T, $\Delta H_y = 0.110(2)$ T, $\Delta H_z = 0.063(2)$ T, $A_x = A_y = 1$, and $A_z = 7.0(5)$. The anisotropic spin-phonon coupling originating from the low-symmetry crystal structure of the present compound is considered to cause the angular dependencies in ΔH. As the transition probability is proportional to the square of the g value in the direction of the oscillating magnetic field, the differences in A are qualitatively consistent with the angular dependencies of the g values.

Next, we examined the evaluated magnetic anisotropy of Co^{2+} in a distorted octahedral environment. The total orbital and spin angular momenta of the high-spin Co^{2+} ion are $L = 3$ and $S = 3/2$, respectively. The ground-state orbital triplet $^4T_1$ in a cubic crystalline electric field is described by $-(3/2)l$ with a fictitious orbital angular momentum $l = 1$. Furthermore, the orbital degeneracy of $^4T_1$ is removed by the axial and rhombic crystal fields, δ_z and δ_{xy}, leading to triaxial magnetic anisotropy. The perturbative treatment of the spin-orbit coupling and crystal fields gives the Hamiltonian as

$$\mathcal{H} = \tfrac{3}{2}\lambda' l\cdot S - \delta_z\left(l_z^2 - \tfrac{2}{3}\right) - \delta_{xy}\left(l_x^2 - l_y^2\right), \tag{5}$$

where $\lambda' = k\lambda$, λ is the spin-orbit coupling constant, and k is the orbital reduction factor originating from the admixture

between the 3*d* electron and *p* electrons in the ligands [32,33]. It is known that typical values of λ and k for a hexa-coordinated high-spin Co^{2+} ion lie in the range -180 to -130 cm^{-1} and 0.6–0.9, respectively [50,51]. Here, we obtained 12×12 matrix elements for the Hamiltonian for $|l_z, S_z\rangle$. The energy states were obtained as a function of δ_z/λ' with the other parameters fixed by numerically solving the secular equation. Because there is an energy gap of several hundred kelvin between the ground Kramers doublet and the first-excited state, the magnetic properties at low temperatures can be described using the doublet state. By applying an external magnetic field, the lowest Kramers doublet $\psi_\pm$ splits because of the Zeeman interaction defined by

$$\mathcal{H}_Z = \mu_B\left(-\tfrac{3}{2}k\boldsymbol{l} + 2\boldsymbol{S}\right)\cdot H. \tag{6}$$

Here, when considering the energy shift of the Kramers doublet as the Zeeman splitting of an effective spin $S_{\rm eff} = 1/2$ (fictitious spin), the g values for the principal axes are given by

$$g_z = \pm 2\langle\psi_\pm|\left(-\tfrac{3}{2}kl_z + 2S_z\right)|\psi_\pm\rangle, \tag{7}$$

$$g_x = \langle\psi_\pm|\left[-\tfrac{3}{2}k(l^+ + l^-) + 2(S^+ + S^-)\right]|\psi_\mp\rangle, \tag{8}$$

$$g_y = \mp\langle\psi_\pm|\left[-\tfrac{3}{2}k(l^- - l^+) + 2(S^- - S^+)\right]|\psi_\mp\rangle, \tag{9}$$

where $l^\pm = l_x \pm i l_y$ and $S^\pm = S_x \pm i S_y$. We explained the anisotropic g values evaluated from the ESR analysis using the parameters $\delta_z/\lambda' = -4.7$, $\delta_{xy}/\lambda' = 0.89$, and $k = 0.61$, as shown in Fig. 6(a). The resulting crystal fields are close to those of similar Co compounds with hfac ligands; the obtained value of k is within the typical range for hexa-coordinated high-spin Co^{2+} complexes [50,51].

Finally, we evaluated the anisotropy of the exchange interaction between S_V on the radicals and $S_{\rm eff}$ on the Co^{2+} ions. Considering the matrix elements of S written as

$$\langle\psi_\pm|S_z|\psi_\pm\rangle = \pm\frac{p}{2}, \quad \langle\psi_\pm|S_x|\psi_\mp\rangle = \frac{q_x}{2},$$
$$\langle\psi_\pm|S_y|\psi_\mp\rangle = \mp i\frac{q_y}{2}, \tag{10}$$

the true spin-3/2 on Co^{2+} is replaced by

$$S_z = pS^z_{\rm eff}, \quad S_x = q_x S^x_{\rm eff}, \quad S_x = q_y S^y_{\rm eff}. \tag{11}$$

Then, the effective exchange interaction between S_V and $S_{\rm eff}$ is expressed as

$$\mathcal{H}_{\rm eff} = J_{\rm eff}\left(S^z_V S^z_{\rm eff} + \epsilon_x S^x_V S^x_{\rm eff} + \epsilon_y S^y_V S^y_{\rm eff}\right), \tag{12}$$

where $\epsilon_x = q_x/p$ and $\epsilon_y = q_y/p$. Assuming the parameters determined using the g values, we obtained ϵ_x and ϵ_y as a function of δ_z/λ', as shown in Fig. 6(b). These results suggest that the present Co-verdazyl complex has an Ising-type anisotropy with $\epsilon_x = 0.44$ and $\epsilon_y = 0.54$. This anisotropic interaction may also affect the magnetization curve in the region below and above the plateau phase.

V. SUMMARY

We successfully synthesized a verdazyl-based complex, (p-Py-V-p-F)$_2$[Co(hfac)$_2$]. The Co atom is coordinated with two p-Py-V-p-F ligands, yielding an octahedral coordination environment. The MO calculations indicated two predominant

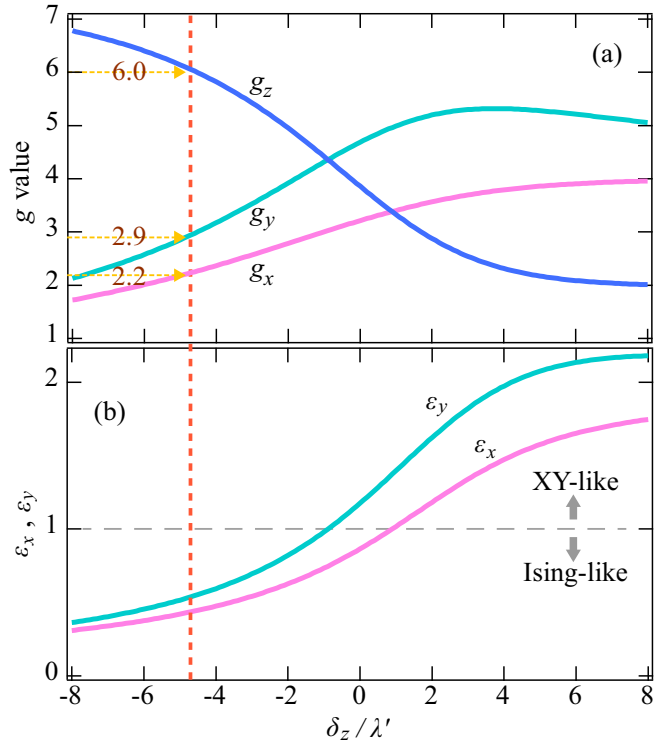

FIG. 6. (a) Anisotropic g values for the ground Kramers doublet of the Co^{2+} ion as a function of δ_z/λ' with $\delta_{xy}/\lambda' = 0.89$ and $k = 0.61$. The inserted g values were obtained from the ESR analysis. The vertical line shows $\delta_z/\lambda' = -4.7$ for the present compound. (b) Expected anisotropy of the effective exchange interaction between the spins on the radical and Co^{2+} ion in the low-temperature region. The horizontal line indicates an isotropic Heisenberg-type with 1.0.

AFM interactions forming a spin-1/2 two-leg spin ladder. Furthermore, the S_V-comprised spin ladders, which originated from the overlapping ligands, connected to the S_{Co} of the Co^{2+} ions via intramolecular interactions to form a ladder-based 2D spin model. The magnetization in the low-field region exhibited paramagnetic behavior associated with the S_{Co} spin. In the high-field region, the S_{Co} spins were fully polarized and resulted in a 3/5 magnetization plateau, indicating the formation of a rung-singlet-like ground state. We calculated the magnetization curve of the spin-1/2 spin ladder by using the QMC method and evaluated the exchange interactions forming the effective spin ladder above the plateau phase. The calculated magnetization curve indicated nonlinear behavior accompanied by a double-peak structure in the field derivatives, which is in clear contrast to the almost linear increase observed in the experimental result. The peculiar behavior of the linear magnetization curve after the magnetization plateau is considered to reflect the nature of the 2D quantum spin system, demonstrating a quantum phase transition from the gapped quantum state to the 2D magnetic state. We also examined the magnetic anisotropy originating from Co^{2+} in a distorted octahedral environment and evaluated the anisotropic g values via ESR powder pattern analysis. Furthermore, considering the spin-orbit coupling and crystal-field distortion of the Co^{2+} ion, we explained the evaluated anisotropic g values of the

effective spin-1/2 on the Co^{2+} ion. The presence of Ising-like exchange interactions between the radical and the effective spins are also expected from the observed crystal-field results.

These results demonstrate that the present ladder-based 2D spin model combines the characteristics of 1D gapped and 2D gapless systems. Considering the variety of molecular structures possible from the combination of verdazyl radicals and Co^{2+} ions, the synthesis method may be utilized to access similar types of spin systems. This work should therefore stimulate the study of quantum many-body phenomena in anisotropic spin models between 1D and 2D systems.

ACKNOWLEDGMENT

A part of this work was performed under the interuniversity cooperative research program of the joint-research program of ISSP, the University of Tokyo.

[1] E. Dagotto and T. M. Rice, Science **271**, 618 (1996).
[2] M. Uehara, T. Nagata, J. Akimitsu, H. Takahashi, N. Mori, and K. Kinoshita, J. Phys. Soc. Jpn. **65**, 2764 (1996).
[3] M. Azuma, Z. Hiroi, M. Takano, K. Ishida, and Y. Kitaoka, Phys. Rev. Lett. **73**, 3463 (1994).
[4] N. D. Mermin and H. Wagner, Phys. Rev. Lett. **17**, 1133 (1966).
[5] M. Matsumoto, C. Yasuda, S. Todo, and H. Takayama, Phys. Rev. B **65**, 014407 (2001).
[6] M. Troyer, M. E. Zhitomirsky, and K. Ueda, Phys. Rev. B **55**, R6117 (1997).
[7] J.-J. Jiang, Phys. A (Amsterdam, Neth.) **540**, 123131 (2020).
[8] S. C. Furuya, M. Dupont, S. Capponi, N. Laflorencie, and T. Giamarchi, Phys. Rev. B **94**, 144403 (2016).
[9] M. Jeong, H. Mayaffre, C. Berthier, D. Schmidiger, A. Zheludev, and M. Horvatić, Phys. Rev. Lett. **118**, 167206 (2017).
[10] D. Macdougal, A. S. Gibbs, T. Ying, S. Wessel, H. C. Walker, D. Voneshen, F. Mila, H. Takagi, and R. Coldea, Phys. Rev. B **98**, 174410 (2018).
[11] B. D. Koivisto and R. G. Hicks, Coord. Chem. Rev. **249**, 2612 (2005).
[12] C. W. Johnston, S. D. J. McKinnon, B. O. Patrick, and R. G. Hicks, Dalton Trans. **42**, 16829 (2013).
[13] T. M. Barclay, R. G. Hicks, M. T. Lemaire, and L. K. Thompson, Inorg. Chem. **40**, 5581 (2001).
[14] S. D. J. McKinnon, B. O. Patrick, A. B. P. Lever, and R. G. Hicks, Inorg. Chem. (Washington, DC, U. S.) **52**, 8053 (2013).
[15] D. J. R. Brook, V. Lynch, C. Conklin, and M. A. Fox, J. Am. Chem. Soc. **119**, 5155 (1997).
[16] H. Yamaguchi, K. Iwase, T. Ono, T. Shimokawa, H. Nakano, Y. Shimura, N. Kase, S. Kittaka, T. Sakakibara, T. Kawakami, and Y. Hosokoshi, Phys. Rev. Lett. **110**, 157205 (2013).
[17] H. Yamaguchi, T. Okubo, K. Iwase, T. Ono, Y. Kono, S. Kittaka, T. Sakakibara, A. Matsuo, K. Kindo, and Y. Hosokoshi, Phys. Rev. B **88**, 174410 (2013).
[18] H. Yamaguchi, H. Miyagai, M. Yoshida, M. Takigawa, K. Iwase, T. Ono, N. Kase, K. Araki, S. Kittaka, T. Sakakibara, T. Shimokawa, T. Okubo, K. Okunishi, A. Matsuo, and Y. Hosokoshi, Phys. Rev. B **89**, 220402(R) (2014).
[19] H. Yamaguchi, T. Okubo, S. Kittaka, T. Sakakibara, K. Araki, K. Iwase, N. Amaya, T. Ono, and Y. Hosokoshi, Sci. Rep. **5**, 15327 (2015).
[20] H. Yamaguchi, Y. Tamekuni, Y. Iwasaki, and Y. Hosokoshi, Phys. Rev. B **97**, 201109(R) (2018).
[21] H. Yamaguchi, Y. Sasaki, T. Okubo, M. Yoshida, T. Kida, M. Hagiwara, Y. Kono, S. Kittaka, T. Sakakibara, M. Takigawa, Y. Iwasaki, and Y. Hosokoshi, Phys. Rev. B **98**, 094402 (2018).
[22] H. Yamaguchi, Y. Iwasaki, Y. Kono, T. Okubo, S. Miyamoto, Y. Hosokoshi, A. Matsuo, T. Sakakibara, T. Kida, and M. Hagiwara, Phys. Rev. B **103**, L220407 (2021).
[23] H. Yamaguchi, Y. Shinpuku, T. Shimokawa, K. Iwase, T. Ono, Y. Kono, S. Kittaka, T. Sakakibara, and Y. Hosokoshi, Phys. Rev. B **91**, 085117 (2015).
[24] H. Yamaguchi, Y. Shinpuku, Y. Kono, S. Kittaka, T. Sakakibara, M. Hagiwara, T. Kawakami, K. Iwase, T. Ono, and Y. Hosokoshi, Phys. Rev. B **93**, 115145 (2016).
[25] H. Yamaguchi, M. Okada, Y. Kono, S. Kittaka, T. Sakakibara, T. Okabe, Y. Iwasaki, and Y. Hosokoshi, Sci. Rep. **7**, 16144 (2017).
[26] N. Uemoto, Y. Kono, S. Kittaka, T. Sakakibara, T. Yajima, Y. Iwasaki, S. Miyamoto, Y. Hosokoshi, and H. Yamaguchi, Phys. Rev. B **99**, 094418 (2019).
[27] Y. Kono, T. Okabe, N. Uemoto, Y. Iwasaki, Y. Hosokoshi, S. Kittaka, T. Sakakibara, and H. Yamaguchi, Phys. Rev. B **101**, 014437 (2020).
[28] Y. Iwasaki, T. Okabe, N. Uemoto, Y. Kono, Y. Hosokoshi, S. Nakamura, S. Kittaka, T. Sakakibara, M. Hagiwara, T. Kawakami, and H. Yamaguchi, Phys. Rev. B **101**, 174412 (2020).
[29] H. Yamaguchi, N. Uemoto, T. Okubo, Y. Kono, S. Kittaka, T. Sakakibara, T. Yajima, S. Shimono, Y. Iwasaki, and Y. Hosokoshi, Phys. Rev. B **104**, L060411 (2021).
[30] H. Tsukiyama, S. Morota, S. Shimono, Y. Iwasaki, M. Hagiwara, Y. Hosokoshi, and H. Yamaguchi, Phys. Rev. Mater. **6**, 094417 (2022).
[31] H. Yamaguchi, S. C. Furuya, S. Morota, S. Shimono, T. Kawakami, Y. Kusanose, Y. Shimura, K. Nakano, and Y. Hosokoshi, Phys. Rev. B **106**, L100404 (2022).
[32] A. Abragam and M. H. L. Pryce, Proc. R. Soc. A **206**, 173 (1951).
[33] M. E. Lines, Phys. Rev. **131**, 546 (1963).
[34] S. K. Satija, G. Shirane, Y. Yoshizawa, and K. Hirakawa, Phys. Rev. Lett. **44**, 1548 (1980).
[35] Y. Nakagawa, T. Kashiwagi, H. Yamaguchi, S. Kimura, Z. Honda, K. Yamada, K. Kindo, and M. Hagiwara, J. Phys. Soc. Jpn. **75**, 124708 (2006).
[36] S. Kimura, H. Yashiro, K. Okunishi, M. Hagiwara, Z. He, K. Kindo, T. Taniyama, and M. Itoh, Phys. Rev. Lett. **99**, 087602 (2007).
[37] A. Arauzo, E. Bartolomé, J. Luzón, P. J. Alonso, A. Vlad, M. Cazacu, M. F. Zaltariov, S. Shova, J. Bartolomé, and C. Turta, Molecules **26**, 5626 (2021).
[38] R. Kuhn, Angew. Chem. **76**, 691 (1964).

[39] M. C. Burla, R. Caliandro, M. Camalli, B. Carrozzini, G. L. Cascarano, L. De Caro, C. Giacovazzo, G. Polidori, and R. Spagna, J. Appl. Crystallogr. **38**, 381 (2005).
[40] G. M. Sheldrick: *SHELXL97, Program for Crystal Structure Determination* (University of Göttingen, Germany, 1997).
[41] M. Shoji, K. Koizumi, Y. Kitagawa, T. Kawakami, S. Yamanaka, M. Okumura, and K. Yamaguchi, Chem. Phys. Lett. **432**, 343 (2006).
[42] A. W. Sandvik, Phys. Rev. B **59**, R14157(R) (1999).
[43] A. F. Albuquerque, F. Alet, P. Corboz, P. Dayal, A. Feiguin, L. Gamper, E. Gull, S. Gurtler, A. Honecker, R. Igarashi, M. Korner, A. Kozhevnikov, A. Lauchli, S. R. Manmana, M. Matsumoto, I. P. McCulloch, F. Michel, R. M. Noack, G. Pawlowski, L. Pollet *et al.*, J. Magn. Magn. Mater. **310**, 1187 (2007).
[44] B. Bauer, L. D. Carr, A. Feiguin, J. Freire, S. Fuchs, L. Gamper, J. Gukelberger, E. Gull, S. Guertler, A. Hehn, R. Igarashi, S. V. Isakov, D. Koop, P. N. Ma, P. Mates, H. Matsuo, O. Parcollet, G. Pawlowski, J. D. Picon, L. Pollet, E. Santos, V. W. Scarola, U. Schollwöck, C. Silva, B. Surer, S. Todo, S. Trebst, M. Troyer, M. L. Wall, P. Werner, and S. Wessel, J. Stat. Mech.: Theory Exp. (2011) P05001.
[45] Y. Shirata, H. Tanaka, A. Matsuo, and K. Kindo, Phys. Rev. Lett. **108**, 057205 (2012).
[46] X. C. Liu, Z. W. Ouyang, T. T. Xiao, J. J. Cao, Z. X. Wang, Z. C. Xia, Z. Z. He, and W. Tong, Phys. Rev. B **105**, 134417 (2022).
[47] Y. Iwasaki, Y. Sasaki, Y. Hosokoshi, A. Matsuo, K. Kindo, and H. Yamaguchi, J. Phys. Soc. Jpn. **88**, 044709 (2019).
[48] K. Okunishi, Y. Hieida, and Y. Akutsu, Phys. Rev. B **60**, R6953 (1999).
[49] N. Maeshima and K. Okunishi, Phys. Rev. B **62**, 934 (2000).
[50] D. V. Korchagin, A. V. Palii, E. A. Yureva, A. V. Akimov, E. Y. Misochko, G. V. Shilov, A. D. Talantsev, R. B. Morgunov, A. A. Shakin, S. M. Aldoshin, and B. S. Tsukerblat, Dalton Trans. **46**, 7540 (2017).
[51] F. Lloret, M. Julve, J. Cano, R. R. Carcía, and E. Pardo, Inorg. Chim. Acta **361**, 3432 (2008).